Photodissociation of pyrrole-ammonia clusters below 218 nm: Quenching of statistical decomposition pathways under clustering conditions

J. D. Rodríguez, M. G. González, L. Rubio-Lago,[a] and L. Bañares[b]
Departamento de Química Física I, Facultad de Ciencias Químicas, Universidad Complutense de Madrid, 28040 Madrid, Spain

(Received 22 June 2012; accepted 17 August 2012; published online 5 September 2012)

The excited state hydrogen transfer (ESHT) reaction in pyrrole-ammonia clusters ($PyH \cdot (NH_3)_n$, $n = 2$–5) at excitation wavelengths below 218 nm down to 199 nm, has been studied using a combination of velocity map imaging and non-resonant detection of the $NH_4(NH_3)_{n-1}$ products. Special care has been taken to avoid evaporation of solvent molecules from the excited clusters by controlling the intensity of both the excitation and probing lasers. The high resolution translational energy distributions obtained are analyzed on the base of an impulsive mechanism for the hydrogen transfer, which mimics the direct N−H bond dissociation of the bare pyrrole. In spite of the low dissociation wavelengths attained (∼200 nm) no evidence of hydrogen-loss statistical dynamics has been observed. The effects of clustering of pyrrole with ammonia molecules on the possible statistical decomposition channels of the bare pyrrole are discussed. © *2012 American Institute of Physics*. [http://dx.doi.org/10.1063/1.4749384]

I. INTRODUCTION

Photodecomposition of pyrrole upon UV radiation absorption is governed by the competition between direct bond cleavage and statistical dissociation producing, in both cases, hydrogen atoms and pyrrolyl radicals.[1] The measurement of the produced hydrogen atom translational energy distribution constitutes a suitable tool to follow the dynamics of both type of dissociation mechanisms. Two well-resolved features can be distinguished in the H-atom translational energy distributions:[2–4] A sharp and structured translational energy distribution, corresponding to *fast* hydrogen atoms produced through direct N−H bond cleavage -direct channel- and a broad and unstructured translational energy distribution corresponding to *slow* hydrogen atoms. The nomenclature *fast* and *slow* refers to the relative position of the peaks − ∼0.85 and ∼0.13 eV, respectively − although the tail of the *slow* Boltzmann-like distribution, that extends beyond the *fast* distribution can be significant in particular conditions.[2] The formation of such *slow* H-atoms has attracted considerable attention in the related literature and several mechanisms have been proposed:[2,5–9] (i) direct excitation to the bound S_2 ($^1B_2$ $^1\pi\pi^*$) state, followed by internal conversion to the ground $\tilde{X}^1A_1$ electronic state, S_0, and statistical dissociation of the hot parent molecules;[2,6] (ii) frustrated dissociation in the repulsive S_1 ($^1A_2$ $^1\pi\sigma^*$) state;[2,6] (iii) resonance-enhanced multiphoton ionization of the parent molecules *via* the $^1\pi\pi^*$ state, followed by dissociation of the ion (dissociative ionization);[7] (iv) ring-opening fragmentation involving C−H bond breaking;[5] (v) adiabatic dissociation in the S_1 ($^1A_2$ $^1\pi\sigma^*$) state.[7,8] Generally speaking, the dissociation dynamics and branching ratio between *fast* and *slow* hydrogen atoms will be governed by the interaction between the three involved states, S_0, S_1, and S_2 at the different excitation energies considered.

Three dynamical regions have been characterized depending on the excitation wavelength. Between 254 nm and 222 nm,[2] the 1^1A_2 $^1\pi\sigma^*$ state − which, unlike for most chromophores, lies at lower energies than the 1^1B_2 state − is directly populated by vibrational coupling with the $^1\pi\pi^*$ state.[2] After absorption, the excited pyrrole molecules evolve on the $^1\pi\sigma^*$ state, towards the curve crossing with the ground state − in the N−H coordinate − from where most molecules proceed non-adiabatically and dissociate asymptotically, producing hydrogen atoms with high translational energy (*fast* hydrogen atoms) and relatively cold pyrrolyl radicals. The structured translational energy distributions reported by Ashfold *et al.*[2] using hydrogen Rydberg atom photofragment translational spectroscopy, indicates that the velocity distribution of those *fast* hydrogen atoms produced at long wavelengths, reflects the vibrational activity of the pyrrolyl co-fragment. Unexpectedly for a molecule with 24 vibrational modes, the analysis of the translational or kinetic energy distributions (KEDs) proved how the pyrrolyl is formed in a limited subset of vibrational states.[4] On the other hand, a fraction of the excited molecules, which are "bounced" in the conical intersection between the $^1\pi\sigma^*$ state and the ground state, should explore the deep well of the ground state potential and undergo substantial intramolecular vibrational energy redistribution (IVR) before unimolecular (statistical) decay occurs (mechanism ii). The randomization of energy would produce in this case *slow* hydrogen atoms and vibrationally hot pyrrolyl radicals.[2]

At higher excitation energies (217 nm $\leq \lambda_{phot} \leq$ 222 nm), the absorption cross section of pyrrole increases considerably due to the onset of the dipole allowed $1^1B_2 \leftarrow \tilde{X}^1A_1$ transition. The excited molecules can decay through fast $S_2 \rightsquigarrow S_1$ radiationless transfer and dissociate in a similar

[a]E-mail: rubio@quim.ucm.es.
[b]E-mail: banares@quim.ucm.es.

way than in the longer wavelength region. The *fast* hydrogen atom KEDs formed through this route would lack of any structure, since the vibrational information related to the promoting modes is lost in the relaxation process.[2] Decay to the ground state by successive $S_2 \rightsquigarrow S_1 \rightsquigarrow S_0$ radiationless transfer steps, and consequent dissociation would result in *slow* hydrogen atoms (mechanism i).[2] Direct excitation to the $^1\pi\pi^*$ state followed by multiphoton ionization enables the possibility of dissociative ionization (mechanism iii) and therefore, the formation of H^+ ions. However, the dependence on the detection wavelength of the hydrogen atoms produced by multiphoton ionization of pyrrole at 243 nm indicates that the majority of hydrogen atoms are released as neutrals.[10]

In the high energy regime ($\lambda_{phot} \leq 217$ nm), excitation of the ring deformation modes opens up an additional dissociation pathway, enabled by conical intersections between the $^1\pi\sigma^*$ and $^1\pi\pi^*$ states, and between the $^1\pi\pi^*$ and the ground electronic states (mechanism iv).[5] The fracture of the aromatic ring produces *slow* hydrogen atoms through direct $S_2 \rightsquigarrow S_0$ transfer followed by C–H bond rupture. The production of hydrogen atoms through mechanisms (i)–(iv) is statistical and hence, a slow dynamics − in the nanosecond regime − is expected. However, Stavros and co-workers,[7,11–13] in a series of time-resolved experiments on the photodissociation of several chromophores at 200 nm have reported the production of *slow* hydrogen atoms in a fast time scale (<200 fs), which in some cases constitute the majority of the *slow* contribution of the KED.[7] Such hydrogen atoms would correspond in the case of pyrrol to the direct N−H bond dissociation channel yielding electronically excited pyrrolyl ($^2\pi$ state) fragments (mechanism *v*). The correlating hydrogen atoms would posses little available energy and then they would contribute to the *slow* component in the KEDs.[8]

In solvation conditions, the distortions suffered by the bare molecule potential energy surfaces (PESs) alter the balance between the different processes − ground state or excited state photodissociation − in a magnitude strongly dependent on the nature and the number of solvent molecules. Molecular clusters, located halfway between isolated and solvated systems, provide the ideal tool to study the solvation effect in a tailored solvent environment. The well-known photostability of the biological systems lies in the thermalizing effect of the surrounding bath on the vibrational excited electronic ground state, which in isolated conditions would lead to statistical decomposition.[6,14] In the same way, photodissociation through direct bond cleavage, closely related to biological damage, shows a strong dependence on the solvent nature.[1,6]

In a recent paper, we have applied the velocity map imaging (VMI) technique to study the photodissociation dynamics of pyrrole-ammonia clusters, $PyH \cdot (NH_3)_n$, in the wavelength interval ranging from 234 to 218 nm.[15] Non-resonant multiphoton ionization (MPI) coupled with the VMI technique provided high resolution translational energy and angular distributions of the cluster $NH_4(NH_3)_m$ ($m = n - 1$) products. The photodynamics of the $PyH \cdot (NH_3)_n$ clusters constitutes a prototypical example of intracluster excited state hydrogen atom transfer (ESHT) reaction,[15,16] where, after one UV photon absorption, the parent clusters decompose into pyrrolyl radicals and $NH_4(NH_3)_m$. The hydrogen transfer is viewed as a bimolecular reaction, where the hydrogen atom ejected by the pyrrole moiety collides and bonds to the nearest NH_3 molecule.[15] The extrapolation of the N−H bond dissociation to the ESHT is not straightforward due to the change of symmetry in the chromophore. In a recent paper, Slavíček and Fárník have analyzed three different hydrogen bond patterns in clusters of N-containing heteroaromatics.[17] In pyrrole clusters, the N−H bond of one molecule binds to the π electron cloud of the neighboring molecule, stabilizing the system due to inhibition of the direct N−H bond dissociation. The same effect has been found in pyrrole—Xe clusters.[17,18] The pyrrole-ammonia N−H bond is more similar to the N−H···N hydrogen bond pattern shown by the imidazole and pyrazole clusters. In this two cases, in a similar way to that of the pyrrole−ammonia clusters, the hydrogen transfer reaction is not quenched by complexation, and results in stable product species. In our previous work,[15] the measured low translational energy distributions of the $NH_4(NH_3)_m$ cluster products were consistent with an impulsive hydrogen atom transfer model, which resembles the bare molecule direct hydrogen atom ejection. These results contradict, however, the electronic mechanism proposed previously by Jouvet and coworkers[16] for the same system, where the high product translational energy measured suggested an electron-proton charge transfer for the $NH_4(NH_3)_m$ species formation.

In the impulsive mechanism proposed in Ref. 15, the pyrrole moiety is excited to a vibrational superposition of S_2 ($^1B_2$ $^1\pi\pi^*$) − S_1 ($^1A_2$ $^1\pi\sigma^*$) states. The hydrogen atoms produced after the direct N−H bond rupture collide with the $(NH_3)_n$ solvent structure forming the $NH_4(NH_3)_m$ products. The velocity distribution of the ejected hydrogen atom correlates with the vibrational activity of the pyrrolyl co-product, which is reflected, in turn, in the $NH_4(NH_3)_m$ KEDs.[15] The effect of microsolvation on the pyrrole PESs became apparent in three experimental facts when compared to the bare molecule case:[15] First, the spectroscopic range where the hydrogen atom transfer was observed is blue shifted by ∼15 nm; second, the coupling between the S_2 and S_1 surfaces involves considerably higher vibrational modes; and third, no evidences of statistical deactivation is found.[15]

The aim of the present work is to study the photodynamics of the $PyH \cdot (NH_3)_n$ clusters, the possible contribution of impulsive or electronic mechanisms and of statistical decomposition pathways, when excitation is produced further to the blue down to ≈200 nm. The main question that must be addressed here is to what extent the statistical hydrogen atom formation observed for the bare pyrrole at high excitation energies (see above) is affected by the clustering conditions. The "low" energy region for the $PyH \cdot (NH_3)_n$ system (from 234 to 218 nm, equivalent to the bare pyrrole dissociation region ranging from 250 to 232 nm) has been the subject of our previous work.[15] Here, we move to higher excitation energies, which are equivalent to excitation energies for which dominant statistical decomposition pathways have been observed for bare pyrrole. An important issue that may interfere with the processes under study is the evaporation of ammonia units out of the excited clusters.[19] We have addressed this issue by carefully controlling the excitation and multiphoton ionization laser intensities to avoid as much as possible evaporation

after cluster excitation. For that purpose, we have used the photodynamics of ammonia clusters as a way to find experimental conditions where evaporation is negligible.

The paper is organized as follows: In Sec. II the experimental methodology is presented. Section III gathers the most relevant experimental results which are then discussed in the same section. Finally, Sec. IV is dedicated to present the most important conclusions of the work.

II. EXPERIMENTAL

The adjustment of the standard VMI technique to the peculiarities of the photodissociation studies of large clusters generated between organic chromophores and solvent molecules has been thoroughly addressed in our previous paper[15] on the photodissociation of $PyH \cdot (NH_3)_n$ clusters which, up to date, constitutes the single report on the application of the VMI technique to ESHT reactions. The whole experiment runs at a repetition rate of 10 Hz. A 3% mixture of NH_3 and He with a stagnation pressure of 1–1.5 bar passes through a bubbler with pyrrole at room temperature and the mixture is expanded via a pulsed nozzle (General Valve Series 9, 0.5 mm diameter orifice) into vacuum. The gas pulse passes through a skimmer (beam dynamics, Standard Model 2, 0.5 mm diameter orifice) and reaches the ionization chamber, where the molecular beam is intersected, in the middle of the electrical plates of a time-of-flight (TOF) mass spectrometer, by the photolysis and probe laser pulses, which are counter propagated to each other. The expansion conditions are critical for the formation of H-bonded complexes. In order to attain the best clustering conditions, the pulsed valve was mounted so it was possible to adjust, from outside the reaction chamber without breaking the vacuum, the distance from the valve orifice to the skimmer and the aperture conditions of the valve, while the mass spectrum was monitored in situ. The configuration of the experimental set-up allows to monitor the mass spectra during the data acquisition. Once the desired conditions were achieved the system was stable few hours, until the sample had to be renewed.

To generate radiation below 218 nm down to 199 nm, a sum-frequency mixing nonlinear crystal is used to combine the fundamental and second harmonic radiation of a Nd:YAG pumped dye laser. The resulting unfocused pump laser was strongly collimated and cleaned in order to have a spot size of about 1 mm^2 of homogeneous intensity ($\sim$10 mJ cm^{-2}). The produced $NH_4(NH_3)_m$ fragments are ionized 40 ns later with a loosely focused (f $\sim$ 60 cm) probe pulse generated by a Nd:YAG laser pumped frequency doubled dye laser. The probe wavelength was set at 333.5 nm. The relatively low values of the ionization potential of the $NH_4(NH_3)_m$ ($m > 2$) radical clusters[20] allow efficient non-resonant ionization with one photon of the 333.5 nm radiation (3.72 eV), while their long lifetimes[21] (of the order of ms) allow the fragments to be ionized using nanosecond pump-and-probe delays and nanosecond laser pulses. The NH_4 and NH_3NH_4 products are characterized by ionization potentials above 3.72 eV, and thus no single probe photon ionization of these species is produced. On the other hand, the lifetime of NH_4 is so short (15 ps) that a pump-and-probe detection of this species is only possible if both laser pulses overlap in time. We have used these two facts to check that multiphoton processes induced by the pump pulse do not contribute to our results.

The ionized products are accelerated by an electric potential of 3.5 kV applied to the repeller plate through a field-free TOF region before hitting impedance matched microchannel plates (MCP) (Chevron configuration, 40 mm diameter). The MCPs can be gated with a high voltage pulse to allow only the ions of interest to be detected. The resulting electron avalanche strikes a phosphor screen (P47), thereby creating the ion image, which is recorded by a CCD camera (SONY 1024 $\times$ 768 pixel) controlled by National Instruments (NI) LabView 7.1 and IMAQ VISION software. The final image is obtained as the sum of around 20 000–100 000 laser shots, depending on the quality of the signal. The calibration of the VMI apparatus was carried out as described in detail in Ref. 15.

III. RESULTS AND DISCUSSION

In this work, we have combined the VMI and MPI techniques to investigate the photodecomposition of $PyH \cdot (NH_3)_n$ clusters in the excitation wavelength interval ranging from 214 to 199 nm for different cluster sizes ($n = 2$–5). The evaporation of ammonia solvent molecules out of the excited cluster is a probable process which may compete and interfere with the processes of interest and, thus, it must be avoided as much as possible. The evaporation of solvent units after UV irradiation in molecular clusters has been investigated to some extent for 1-naphtol-$(NH_3)_n$ by Jouvet and co-workers[19] and the main conclusions extracted there are applicable to other chromophore-ammonia clusters. Two main facts were found in that study. First, ammonia evaporation, as a dissociating event, adds an extra amount of translational energy to the cluster products. If evaporation occurs, the translational energy released in the process should appear as an extra contribution in those clusters which undergo evaporation, and the experimental quantification of the evaporation process would require a detailed analysis of the translational energy distribution of the evaporating species. In TOF techniques, the extra translational energy is observed as a broadening of the TOF profiles or, when evaporation from a large number of cluster is summed, a broad and low-intensity background. The conversion of the peak broadening to translational energy requires a non-evaporating reference peak, or a detailed calibration of the TOF apparatus.[19] Second, ammonia evaporation might happen in the first excited state, S_1, in the ionic state, or in both. According to the proposed model in Ref. 19, evaporation in the ion would happen provided that the excess of energy exceeds the binding energy of the ammonia moiety to the parent cluster ion. In this case, the parent transient will show no dynamics (step function). Evaporation might happen in S_1, if the excess of energy provided by the excitation photon is distributed before the ionization step by fast IVR leading to hot clusters. The parent transient will show in this case the evaporation decay dynamics.

In order to quantify the degree of evaporation in the present case and to find the best experimental conditions with minimum evaporation, we have carried out a preliminary

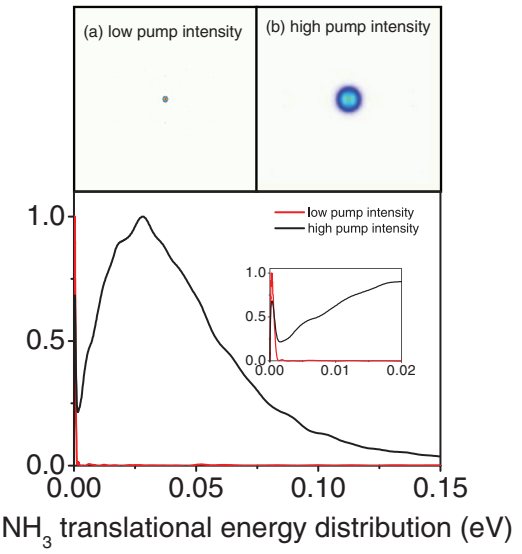

FIG. 1. NH_3^+ images and the corresponding translational energy distributions obtained after two-color irradiation of a pure ammonia cluster beam at (a) low and (b) high intensities of the pump (excitation) laser. See text for details.

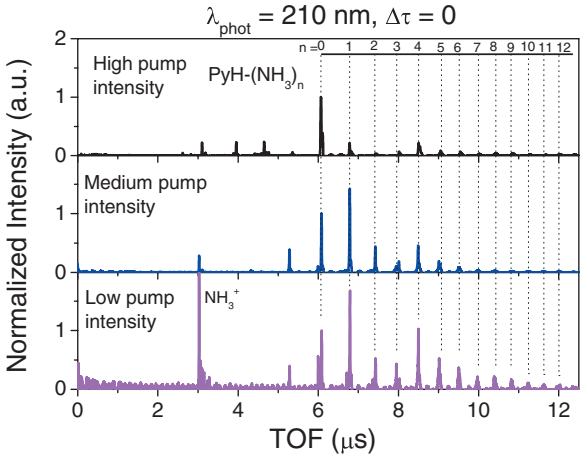

FIG. 2. Zero pump-probe time-of-flight mass spectra obtained at different pump laser intensities and the same expansion conditions. In the lowest pump laser intensity spectrum, the parent cluster distribution is apparent up to $n = 12$, while at the highest pump laser intensity spectrum (top panel), the parent cluster distribution is overcome by the monomer.

study using the same pump and probe lasers but in an molecular beam of ammonia clusters. The excitation and detection wavelengths were set to 210 nm and 333.5 nm, respectively, and the delay between both lasers was set to zero. Two conditions for the pump laser intensity were chosen. A low intensity condition,[22] where no single ammonia or ammonia cluster signals were observed when either one of the pump or probe lasers were blocked, and a high intensity condition, where the pump laser generates a distribution of ammonia and ammonia cluster ions which is significantly enhanced when the probe laser is on. Since the ammonia ionization potential is 10.17 eV,[23] a photon from the pump laser and two photons from the probe laser are needed to produce the ionization (by a $1+2'$ MPI process), while the absence of single laser contribution ensures that no more photons are involved.[24]

Figure 1 shows NH_3^+ images and the corresponding translational energy distributions obtained at the two intensity conditions of the pump laser mentioned above. At low pump laser intensity, the image consists in a spot in the center indicating no recoil. At high pump laser intensity, the NH_3^+ spot is overcome by an unstructured feature with considerable recoil. A non-zero recoil feature is a signature of dissociating dynamics (ammonia evaporation in this case), where the photon energy is partially transferred to the products. Without a detailed energy balance,[25] it is not possible to determine from the images if the dissociation happens on the S_1 or ionic states of the clusters. However, since the only effect of the probe laser pulse is to produce an enhancement of the NH_3 signal under the high pump laser intensity conditions, and such enhancement disappears when a time delay is introduced between the pump and probe pulses − i.e., no dynamics is observed − we conclude that the image shown in Fig. 1(b) reflects the dissociation − evaporation − of one or more ammonia units in the parent ion. By choosing the laser intensity conditions corresponding to the ammonia image with no recoil, we guarantee that evaporation is diminished or completely avoided.

With this information in mind, we have proceeded to study the $PyH \cdot (NH_3)_n$ parent cluster distribution at each photodissociation wavelength employed, i.e., 214, 210, 205, and 199 nm. Figure 2 shows the $PyH \cdot (NH_3)_n$ mass spectra obtained at 210 nm and zero time delay with respect to the probe laser at 333.5 nm, for three different pump laser intensities (similar mass spectra were obtained at the other excitation wavelengths). The spectra have been normalized to the $n = 0$ peak (pyrrole) for comparison. The mass spectrum obtained at the lower pump laser intensity (lower panel) presents a bimodal distribution peaking at $n = 1$ and $n = 4$, although clusters up to $n = 12$–13 are distinguishable. When the pump laser intensity is increased (middle panel), the major difference observed − besides the monomer/cluster ratio − is the weakening of the high-masses part ($n > 6$) of the spectrum. At the highest intensity employed (upper panel), the cluster distribution is barely visible when compared to the bare pyrrole signal. These results are in agreement with the previous discussion about 1-naphtol-$(NH_3)_n$ and with the work of Fárník and co-workers,[17,26–29] who have shown how the MPI mass spectra can lead to a wrong evaluation of the cluster size distribution due to the possible cluster fragmentation upon ionization. The $PyH \cdot (NH_3)_n$ ionization thresholds are expected to lie at lower values than that of the bare molecule − to our knowledge they have not been experimentally determined − and show a stabilization trend above $n \sim 10$.[30] Considering the bare pyrrole IP (8.21 eV)[10] as an upper limit, at zero pump-probe delay the excitation provides enough energy to ionize any $PyH \cdot (NH_3)_n$ cluster present in the molecular beam. To ensure minimal evaporation conditions, the pump laser intensity was regulated in such a way that no recoil was observed when monitoring NH_3^+ images. In the rest of the paper, these experimental conditions were kept to guarantee that evaporation was negligible. When enough large time delay (≈40 ns) is introduced between the pump and probe laser pulses, the $NH_4(NH_3)_{m=2-4}$ products dominate the mass spectra, although some contribution from higher masses (up to $m = 6$) is visible.

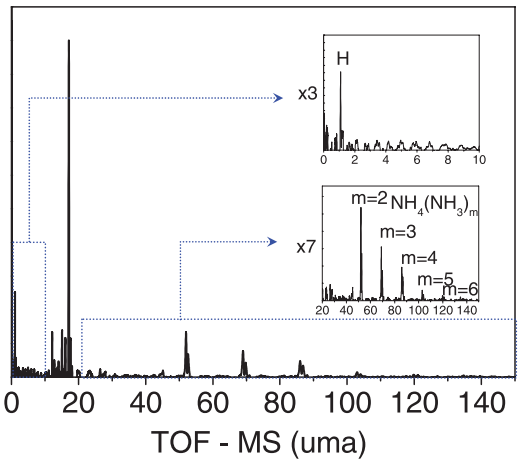

FIG. 3. Difference between the 40 ns and zero delay pump-and-probe time-of-flight mass spectra obtained at the photolysis wavelength of 199 nm. The difference spectrum is dominated by the NH_3 contribution. The insets show the low mass (up) and high mass (down) regions, where the hydrogen atom and the $NH_4(NH_3)_m$ cluster products up to $m = 6$ can be observed, respectively.

Strikingly, no significant amounts of hydrogen atoms are observed in the mass spectra in any condition studied in this work. Since the IP of ammonia and atomic hydrogen are almost equal − 10.17 and 10.2 eV, respectively − a comparable ionization cross section for a (1+2′) MPI process is expected for both species[27] and, hence, the ratio H/NH_3 can be considered as a hydrogen atom production rate. To check that we were able to detect hydrogen atoms, a set of mass spectra was recorded using very high pump intensities. At zero time delay, the dominant peak corresponding to NH_3^+ overwhelms the spectra, although a weak $PyH \cdot (NH_3)_n^+$ progression with $n = 2-6$ can be observed. When the delay is increased to 40 ns, the NH_3^+ contribution is only slightly enhanced, indicating that the major NH_3^+ source is non-resonant MPI induced by the pump pulse. In Figure 3, the difference between the 40 ns and the zero delay pump-and-probe mass spectra is plotted corresponding to a pump laser wavelength of 199 nm. As can be seen, together with the NH_3 peak, the $NH_4(NH_3)_m$ cluster products, up to $m = 6$ are visible in the same vertical scale. Only a small amount of H^+ appears in the delayed mass spectrum, indicating that the hydrogen atoms are produced as neutrals.[10]

Figure 4 shows the $NH_4(NH_3)_2$ raw VMI image obtained at the excitation wavelength of 214 nm, at low pump laser intensities (no evaporation conditions). Similar images, consisting of a single low-recoil isotropic feature, were obtained at each of the photolysis wavelength employed in this work. The translational energy distributions obtained by angular integration of the $NH_4(NH_3)_2$ product images at the different photolysis wavelengths studied are presented in Figure 5. All the distributions show a similar profile, consisting of a Boltzmann-like envelope with a resolved structure around the maximum (located at ∼0.01 eV), and a tail lasting several tens of meV. As the photolysis wavelength is decreased from 214 nm to 199 nm, the structure is compressed in the early part of the distribution. Figure 6 shows the KEDs corresponding to the fragments $NH_4(NH_3)_m$ for $m = 2$, 3, 4 at the fixed photolysis wavelength of 214 nm. The distributions present the same main features in all cases, but the vibrational structure appears significantly blurred due to the larger masses. Although in the mass spectra $NH_4(NH_3)_m$ products up to $m = 6$ are visible, the signal of the higher masses was too low to provide reliable translational energy distributions.

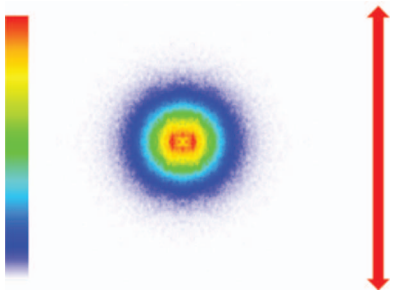

FIG. 4. VMI raw image corresponding to $NH_4(NH_3)_2$ products formed in the photodissociation of $PyH \cdot (NH_3)_3$ at a photolysis wavelength of 214 nm. The double headed arrow denotes the polarization direction of both pump and probe laser pulses.

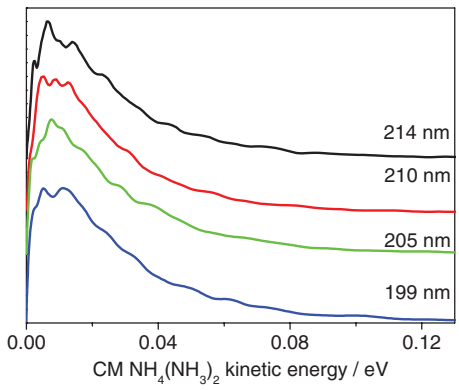

FIG. 5. Translational energy distributions obtained by integration of the Abel inverted images corresponding to the $NH_4(NH_3)_2$ fragment taken at the different photolysis wavelengths employed in the present study. The distributions have been vertically shifted for a clear comparison.

The image shown in Figure 4 and the translational energy distributions of Figures 5 and 6 closely resemble the results obtained in our previous work[15] at excitation wavelengths ranging from 234 to 218 nm. This fact suggests that a single dynamics is responsible for the $NH_4(NH_3)_m$ product

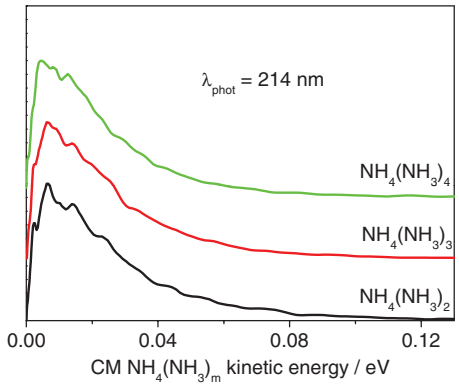

FIG. 6. Center-of-mass (CM) translational energy distributions obtained by integration of the Abel inverted images corresponding to the $NH_4(NH_3)_m$ for $m = 2$, 3, 4 fragments at a fixed photolysis wavelength of 214 nm. The distributions have been vertically shifted for a clear comparison.

formation from 234 nm to 199 nm. To check the consistency of this asset we have analyzed the present data in the same way as in Ref. 15.

The detailed analysis of the internal energy distribution of the particular $NH_4(NH_3)_2$ product is carried out using a *x*-axis normalization: For each photolysis wavelength, the abscissa axis of the translational energy distributions depicted in Figure 5 is divided by the corresponding available energy, as shown in Figure 7. The available energy for each $NH_4(NH_3)_m$ cluster product has been calculated according to the impulsive model − which has been proved to be valid between 234 and 218 nm[15] − which considers the hydrogen atom transfer as a bimolecular reaction between the pyrrole and the $(NH_3)_n$ chain. The translational energy of the ejected hydrogen atom − which carries out the information about the pyrrole vibrational modes involved in the photoexcitation step − is transformed into translational and internal energy of the $NH_4(NH_3)_m$ product,

$$E^{av}[NH_4(NH_3)_m] = \frac{m_H}{m_{NH_4(NH_3)_m}} E^{av}(H), \quad (1)$$

where m_i denotes the mass of the corresponding *i* species, and $E^{av}(H)$ is the available energy for the ejected hydrogen atom given by

$$E^{av}(H) = \frac{m_{Py}}{m_{PyH}}[h\nu - D_0], \quad (2)$$

where $h\nu$ is the energy of the excitation photon and $D_0 = 4.073$ eV is the N−H bond dissociation energy.[2] In the bare pyrrole dissociation the translational energy of the exerted hydrogen atom is quantified and reflects the vibrational coupling between the $^1\pi\pi^*$ and $^1\pi\sigma^*$ states, which is restricted to one quanta in the so-called promoting modes.[4] As mentioned before, the photochemistry of chromophore-ammonia clusters, although closely follows the photochemistry of the bare chromophore, presents some important differences due to the action of the environment on the involved PESs.[6] In the case of the pyrrole-ammonia clusters, the major effect is an increase of the gap between the $^1\pi\pi^*$ and $^1\pi\sigma^*$ states, which modifies their coupling strength and alters the dependence of the parent $PyH\cdot(NH_3)_n$ photodissociation on the excitation energy.[16] Due to this shift, the vibrational coupling between the $^1\pi\pi^*$ and $^1\pi\sigma^*$ states involves higher vibrational levels and hence, higher excitation energies.[15] Such conclusion is in agreement with the experimental threshold obtained for the ESHT reaction at 236.6 nm, around 15 nm lower than the threshold for the fast hydrogen atom formation in the bare molecule.[15,31] According to the impulsive model, the structure of the translational energy distributions of the products is ascribed to vibrational activity in the pyrrolyl radical.[15] The spacing between the major features in the cluster products translational energy distributions observed in Ref. 15 suggested that there are two main vibrational modes of the pyrrolyl radical involved,[2,15] with energies around 3000 cm^{-1} and 1500 cm^{-1}. According to the electric dipole selection rules, which ensure that the initial excitation can only populate levels of a_2, b_1, and b_2 vibrational symmetry − in Herzberg notation[32] −, four vibrational modes, ν_{12} and ν_{13} with values of ∼3200 cm^{-1}, and ν_{14} and ν_{15} with values of ∼1300 cm^{-1}, were considered.[2,15]

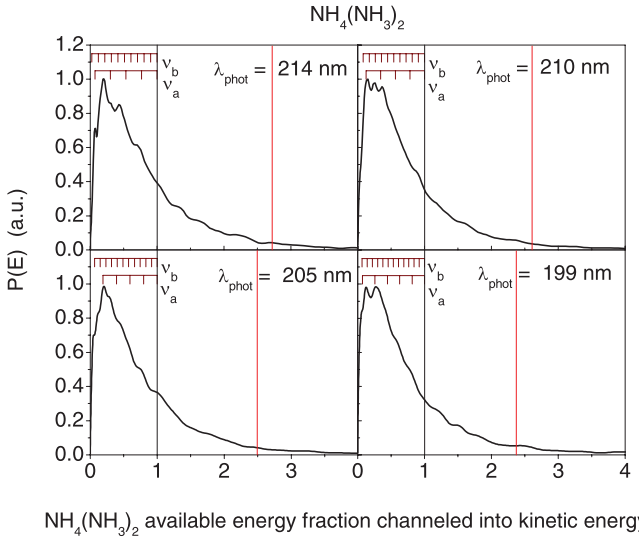

FIG. 7. Center-of-mass (CM) translational energy distributions of the $NH_4(NH_3)_2$ clusters as a function of the available energy fraction channeled into translational energy of the products. The black vertical line corresponds to the maximum fraction of available energy, and correlates with species with zero internal energy. The observed structure has been assigned to the vibrational activity of the pyrrolyl radical. As a visual guide, the combs corresponding to generic vibrational quantum states of 3000 cm^{-1} (ν_a) and 1500 cm^{-1} (ν_b) modes of the pyrrolyl co-fragment moiety have been included (top of each panel). The tail in the translational energy distribution extending towards values larger than one is related to internal energy of the ammonia chains. The vertical red lines correspond to the available energy if a quantum of the intermolecular bending mode of 452 cm^{-1} is included (see text for details).

In order to compare the present results with our previous work, and without the aim of performing any rigorous vibrational assignment, vibrational combs of 3000 cm^{-1} (ν_a) and 1500 cm^{-1} (ν_b) are included in Figure 7.

As the photolysis wavelength decreases, the corresponding increase of the available energy should imply a broadening of the translational energy distribution.[15] However, when the photolysis wavelength is varied from 214 to 199 nm, the opposite behavior is observed. Furthermore, when compared the translational energy distributions of the $NH_4(NH_3)_m$ clusters obtained in the present work (Fig. 7) with those obtained between 234 and 218 nm (Fig. 9 in Ref. 15) is clear that a loss in the structure resolution is produced at lower wavelengths. The lack of structure involving higher vibrational excitation suggests a weakening of the vibrational coupling between the $^1\pi\pi^*$ and $^1\pi\sigma^*$ states as expected,[5,6] and a probable contribution of ESHT triggered by "fast" hydrogen atoms produced after direct excitation to the $^1\pi\pi^*$ state.[2] The portion of the curves at the right side of the available energy black bar in Figure 7 corresponds to internal energy of the ammonia chain (which is not taken into account in Eq. (1)). The $NH_4(NH_3)_{m-1}$ $-NH_3$ binding energies lie above 0.2 eV for $m \geq 3$ (Ref. 20). Considering that the translational energy distributions depicted in Figure 5 do not extend beyond ∼0.12 eV (970 cm^{-1}), it is clear that while the $NH_4(NH_3)_m$ clusters do not posses enough energy to decompose spontaneously, the excess energy can be used to populate intracluster vibrational and rotational modes (between 18 and 452 cm^{-1}).[33] The red vertical lines in Figure 7 represent the

available energy if one quanta of the intermolecular bending mode (452 cm^{-1}) is considered.

Interestingly, the present results also confirm that no evidence of the electronic mechanism proposed by Jouvet and co-workers.[16] is found at excitation wavelengths as short as 199 nm.

In the previous discussion the parallelism between the direct N−H bond dissociation in the bare molecule, and the ESHT reaction in the cluster has been established, i.e., the *fast* hydrogen atom production is traduced to a hydrogen transfer reaction. The question that must be addressed now is how does the ammonia solvent affects the *slow* hydrogen atom dynamics. Since the increase of the gap between the $^1\pi\pi^*$ and $^1\pi\sigma^*$ states is mainly due to a stabilization of the $^1\pi\sigma^*$ state, the coupling between the $^1\pi\pi^*$ state and the ground state at high energies should not depend significatively on the solvent. In other words, independently of the effect of the ammonia molecules on the N−H bond dissociation, the internal conversion from the $^1\pi\pi^*$ state to the ground state, one of the main sources of statistical hydrogen atom formation, should remain unaltered.[6,26] Furthermore, assuming that the 15 nm difference between the absorption onsets of pyrrole and pyrrole-ammonia measured previously,[15,16] stands at these wavelengths, at 199 nm the ring deformation channel should be open, adding an extra contribution to the slow hydrogen atom branching ratio through C–H bond rupture.[5] However, the fact that no abundant hydrogen atoms have been detected in the MPI mass spectra recorded in the present work are against these expectations. Our results indicate that interactions between the different PESs are affected by clustering with ammonia molecules in a greater extent than expected. The main effect is an apparent weakening of the non-radiative transfer processes ($S_2 \rightsquigarrow S_0$ or S_1 and $S_2 \rightsquigarrow S_1 \rightsquigarrow S_0$) with respect to the $^1\pi\pi^* - {}^1\pi\sigma^*$ vibrational coupling. In other words, the mechanisms leading to the statistical production of hydrogen atoms are unbalanced − or *quenched* − with respect to direct dissociation dynamics, under clustering conditions. We would like to point out that these results are restricted to a low clustering degree, where pyrrole interacts with few ammonia molecules. Once the contribution from larger clusters has been minimized by avoiding ammonia evaporation, as explained in the text, no cluster contribution above $n = 5$ is assumed. Since it is well known that in solvated conditions direct bond dissociation is strongly quenched so it cannot compete with the relaxation processes, our results suggest that either an intermediate clustering range − between n∼5 and full solvation −, where ESHT and relaxation processes compete, or a sharp threshold for the ESHT quenching, must exist.

It must be stated that the lack of statistical hydrogen atoms in the photodecomposition of pyrrole-ammonia clusters is in partial disagreement with the observations of Fárník *et al.* related to clusters of imidazole[17,27] and pyrazole,[17] despite the similarity of the hydrogen bonding pointed out above. In the photodissociation of these systems, the slow component of the hydrogen atom kinetic energy distributions increases with complexation and dominates even at 193 nm, where direct excitation to the $\pi\pi^*$ state occurs. However, the overall hydrogen atom signal decreases with both cluster size and excitation energy, what is in agreement with our work. Moreover, these authors have found similar results for pyrrole and clusters of pyrrole, imidazole and pyrazole with Ar,[26] where the hydrogen atom of one unit is linked to the π ring of a neighbour.

The clarification of these issues requires additional theoretical calculations, involving parameters such as cluster size, excitation energy and hydrogen bond polarity.

IV. CONCLUSIONS

The photodynamics of the hydrogen atom transfer reaction in pyrrole-ammonia clusters have been study between 214 and 199 nm in velocity map imaging experiments in combination with nonresonant ionization detection of the $NH_4(NH_3)_{m=2-4}$ radical products. The structured product translational energy distributions mimic the results obtained in our previous work at lower excitation energies[15] and, consistently, the same dynamics is proposed: N−H bond dissociation of the pyrrole moiety results in a fast hydrogen atom which collides with the ammonia chain. The observed structure is associated to a discrete velocity distribution of the colliding H-atom which, in turn, reflects the vibrational activity of the pyrrolyl radical, formed in the photodissociation step. No clear sign of hydrogen atom formation has been found. Our results open new questions which need additional experimental and theoretical work to be answered. The lack of statistical hydrogen atoms should be related to a quenching of the statistical decomposition pathways under clusterization. However, according to theoretical calculations, the only channel affected by complexation should be the frustrated $^1\pi\sigma^* - S_0$ curve crossing. If so, this source of statistical hydrogen atoms might be much more relevant than the others, even at these dissociation wavelengths.

ACKNOWLEDGMENTS

J.D.R. acknowledges financial support from MICINN (Spain) through a FPI fellowship. M.G.G. and L.R.-L. thank to MICINN for predoctoral and postdoctoral contracts, respectively, through the Consolider program "Science and Applications of Ultrafast Ultraintense Lasers," Grant No. CSD2007-00013. This work has been financed by the Spanish MICINN through Grant Nos. CTQ2008-02578 and CSD2007-00013. The facilities provided by the Centro de Asistencia a la Investigación de Espectroscopia Multifotónica y de Femtosegundos (UCM) are gratefully acknowledged.

[1] M. N. R. Ashfold, G. A. King, D. Murdock, M. G. D. Nix, T. A. A. Oliver, and Alan G. Sage, Phys. Chem. Chem. Phys. **12**, 1218 (2010).
[2] B. Cronin, M. G. D. Nix, R. H. Qadiry, and M. N. R. Ashfold, Phys. Chem. Chem. Phys. **6**, 5031 (2004).
[3] J. Wei, A. Kuczmann, J. Riedel, F. Renth, and F. Temps, Phys. Chem. Chem. Phys. **5**, 315 (2003).
[4] M. N. R. Ashfold, B. Cronin, A. L. Devine, R. N. Dixon, and M. G. D. Nix, Science **312**, 1637 (2006).
[5] M. Barbatti, M. Vazdar, A. J. A. Quino, M. Eckert-Maksić, and H. Lischka, J. Chem. Phys. **125**, 164323 (2006).
[6] A. L. Sobolewski, W. Domcke, C. Dedonder-Lardeux, and C. Jouvet, Phys. Chem. Chem. Phys. **4**, 1093 (2002).
[7] C. A. Williams, G. M. Roberts, H. Yu, N. L. Evans, S. Ullrich, and V. G. Stavros, J. Phys. Chem. A **116**, 2600 (2012).

[8]V. Vallet, Z. G. Lan, S. Mahapatra, A. L. Sobolewski, and W. Domcke, J. Chem. Phys. **123**, 144307 (2005).
[9]M. Barbatti, J. Pittner, M. Pederzoli, U. Werner, R. Mitrić, V. Bonačić-Koutecký, and H. Lischka, Chem. Phys. **375**, 26 (2010).
[10]A. J. van den Brom, M. Kapelios, T. N. Kitsopoulos, N. H. Nahler, B. Cronin, and M. N. R. Ashfold, Phys. Chem. Chem. Phys. **7**, 892 (2005).
[11]A. Iqbal, L.-J. Pegg, and V. G. Stavros, J. Phys. Chem. A **112**, 9531 (2008).
[12]A. Iqbal, M. S. Y. Cheung, M. G. D. Nix, and V. G. Stavros, J. Phys. Chem. A **113**, 8157 (2009).
[13]A. Iqbal and V. G. Stavros, J. Phys. Chem. A **114**, 68 (2010).
[14]Z. Lan and W. Domcke, Chem. Phys. **350**, 125 (2008).
[15]L. Rubio-Lago, G. A. Amaral, A. N. Oldani, J. D. Rodríguez, M. G. González, G. A. Pino, and L. Bañares, Phys. Chem. Chem. Phys. **13**, 1082 (2011).
[16]O. David, C. Dedonder-Lardeux, C. Jouvet, H. Kang, S. Martrenchard, T. Ebata, and A. L. Sobolewski, J. Chem. Phys. **120**, 10101 (2004).
[17]P. Slavíček and M. Fárník, Phys. Chem. Chem. Phys. **13**, 12123 (2011).
[18]L. Rubio-Lago, D. Zaouris, Y. Sakellariou, D. Sofikitis, T. N. Kitsopoulos, F. Wang, X. Yang, B. Cronin, A. L. Devine, G. A. King, M. G. D. Nix, M. N. R. Ashfold, and S. S. Xantheas, J. Chem. Phys. **127**, 064306 (2007).
[19]C. Deonder-Lardeux, D. Grosswasser, C. Jouvet, S. Matrenchard, and A. Teahu, Phys. Chem. Chem. Phys. **3**, 4316 (2001).
[20]K. Fuke, R. Takasu, and F. Misaizu, Chem. Phys. Lett. **229**, 597 (1994).
[21]K. Fuke and R. Takasu, Bull. Chem. Soc. Jpn. **68**, 3309 (1995).
[22]The high and low intensity conditions involved pulses of $\sim$1 mJ and $<$100 μJ, respectively. The 100 μJ represent the threshold for where no recoil in the NH_3 where found.
[23]S. T. Ceyer, P. W. Tiedmann, B. H. Mahan, and Y. T. Lee, J. Chem. Phys. **70**, 14 (1979).
[24]F. Misaizu, P. L. Houston, N. Nishib, H. Shinohara, T. Kondow, and M. Kinoshita, J. Chem. Phys. **98**, 336 (1993).
[25]To perform a detailed energy balance, additional information must be obtained, in particular the ionization potentials of the parent clusters, and an estimation of the number of ammonia moieties evaporated. However, in the present work we seek to obtain phenomenological conditions where no evaporation takes place and then, such characterization lies out of the scope of our work.
[26]V. Poterya, V. Profant, M. Fárník, P. Slavíček, and U. Buck, J. Chem. Phys. **127**, 064307 (2007).
[27]V. Poterya, V. Profant, M. Fárník, L. Šištík, P. Slavíček, and U. Buck, J. Phys. Chem. A **113**, 14583 (2009).
[28]M. Fárník, V. Poterya, O. Votava, M. Ončák, P. Slavíček, I. Dauster, and U. Buck, J. Phys. Chem. A **113**, 7322 (2009).
[29]V. Poterya, O. Tkac, J. Fedor, M. Fárník, P. Slavíček, and U. Buck, Int. J. Mass. Spectrum. **290**, 85 (2010).
[30]A. Carrera, I. B. Nielsen, P. Carcabal, C. Dedonder, M. Broquier, C. Jouvet, W. Domcke, and A. L. Sobolewski, J. Chem. Phys. **130**, 024302 (2009).
[31]O. David, C. Dedonder-Lardeux, and C. Jouvet, Int. Rev. Phys. Chem. **21**, 499 (2002), and references therein.
[32]G. Herzberg, *Molecular Spectra and Molecular Structure. III. Electronic Spectra and Electronic Structure of Polyatomic Molecules* (Van Nostrand, New York, 1966).
[33]K. Nonose, T. Taguchi, F. Chen, S. Iwata, and K. Fuke, J. Phys. Chem. A **106**, 5242 (2002).